Electrodynamic properties of the semimetallic Dirac material $SrMnBi_2$: Two-carrier-model analysis

H. J. Park,[1,2] Byung Cheol Park,[1,2] Min-Cheol Lee,[1,2] D. W. Jeong,[1,2] Joonbum Park,[3] Jun Sung Kim,[3,4] Hyo Seok Ji,[5] J. H. Shim,[5,6] K. W. Kim,[7] S. J. Moon,[8] Hyeong-Do Kim,[1,2] Deok-Yong Cho,[1,2,9] and T. W. Noh[1,2,*]

[1]*Center for Correlated Electron Systems, Institute for Basic Science (IBS), Seoul 08826, Republic of Korea*

[2]*Department of Physics and Astronomy, Seoul National University, Seoul 08826, Republic of Korea*

[3]*Department of Physics, Pohang University of Science and Technology, Pohang 37673, Republic of Korea*

[4]*Center for Artificial Low Dimensional Electronic Systems, Institute for Basic Science (IBS), Pohang 37673, Korea*

[5]*Department of Chemistry, Pohang University of Science and Technology, Pohang 37673, Republic of Korea*

[6]*Division of Advanced Nuclear Engineering, Pohang University of Science and Technology, Pohang 37673, Republic of Korea*

[7]*Department of Phyisics, Chungbuk National University, Cheongju 28644, Republic of Korea*

[8]*Department of Physics, Hanyang University, Seoul 04763, Republic of Korea*

[9]*IPIT & Department of Physics, Chonbuk National University, Jeonju 54896, Republic of Korea*

(Received 21 April 2017; revised manuscript received 11 September 2017; published 26 October 2017)

The electrodynamics of free carriers in the semimetallic Dirac material $SrMnBi_2$ was investigated using optical spectroscopy and first-principles calculations. Using a two-carrier-model analysis, the total free-carrier response was successfully decomposed into individual contributions from Dirac fermions and non-Dirac free carriers. Possible roles of chiral pseudospin, spin-orbit interaction (SOI), antiferromagnetism, and electron-phonon (e-ph) coupling in the Dirac fermion transport were also addressed. The Dirac fermions possess a low scattering rate of $\sim$10 meV at low temperature and thereby experience coherent transport. However, at high temperatures, we observed that the Dirac fermion transport becomes significantly incoherent, possibly due to strong e-ph interactions. The SOI-induced gap and antiferromagnetism play minor roles in the electrodynamics of the free carriers in $SrMnBi_2$. We also observed a seemingly optical-gap-like feature near 120 meV, which emerges at low temperatures but becomes filled in with increasing temperature. This gap-filling phenomenon is ascribed to phonon-assisted indirect transitions promoted at high temperatures.

DOI: 10.1103/PhysRevB.96.155139

I. INTRODUCTION

Recently, Dirac materials such as graphene [1–3] and topological insulators (TIs) [4–6] have attracted attention due to their linear energy-momentum dispersion. Such linear states in solids can provide a model platform for exploring relativistic Dirac physics and intriguing quantum phenomena such as (anomalous) quantum Hall effects [7–12]. Charge carriers in the linear state are called Dirac fermions, whose electrodynamics can be described with a relativistic Dirac theory instead of a nonrelativistic Schrödinger equation [1–12]. Among various physical properties, the outstanding transport capability of Dirac fermions potentially holds promise for realizing high-speed electronic devices [13,14]. In particular, the ultrahigh mobility of carriers in graphene and TIs, associated with the chirality (or helicity) of their Dirac fermions [2,3,5,6], enhances the feasibility of applying these materials to novel devices. In this context, the investigation of the low-energy Dirac fermion dynamics is important for both fundamental studies and practical applications.

Free-carrier electrodynamics can be investigated using low-energy optical probes, such as terahertz and Fourier-transform infrared (FTIR) spectroscopy [15,16]. These methods measure the light absorption by free carriers in the medium, which results in the characteristic spectral feature, called the Drude peak, in the low-energy optical spectra [15,16]. The Drude feature provides the low-energy electrodynamic properties of free carriers, including scattering rate, direct current (dc) limit of conductivity, and mobility [15,16]. Moreover, the optical methods are usually contact free, nondestructive, and bulk sensitive. Accordingly, they are not susceptible to the experimental difficulties inherent in transport and angle-resolved photoemission spectroscopy (ARPES) measurements [15,16].

Here, using FTIR spectroscopy, we studied low-energy optical properties of $SrMnBi_2$, where a highly anisotropic Dirac-like state and other semimetallic states appear [17–24]. Free carriers in $SrMnBi_2$ can be influenced by strong spin-orbit interactions (SOIs), antiferromagnetic ordering, and strong electron-phonon (e-ph) interactions [17–24]. In particular, Dirac fermions in $SrMnBi_2$ are expected to have interesting properties, such as high mobility and small SOI-induced energy gap [18,21–23]. However, for the band structure [18,22,23], the low-energy electrodynamics of pure Dirac fermions has remained unexplored. Lack of understanding probably originates from the coexistent semimetallic states near the Fermi energy E_F, which hamper the separation of the Dirac fermions from total electrodynamic response [18,22,23]. Additionally, the involvement of other degrees of freedom, such as magnetism and phonons in $SrMnBi_2$, further complicates such studies. In detail, the antiferromagnetism can break the time-reversal symmetry and the e-ph interaction can increase the phase space of the scatterings of Dirac fermions.

Our two-carrier-model analysis will be particularly useful for $SrMnBi_2$, where the scattering rates of two types of carriers are significantly different. Note that the Dirac fermions possess a highly suppressed scattering rate by spin-forbidden backscattering [17], while the non-Dirac free carriers offer a much broader Drude form. Given that the width of a Drude peak is proportional to the scattering rate [15], the spectral

*Corresponding author: twnoh@snu.ac.kr

features of the two free carriers could be well separated in different spectral regions. The optical responses of the two bands (i.e., Dirac and semimetallic bands) satisfy the fundamental relationships given below [15,16]:

$$\omega_p^2 = \omega_{p,n}^2 + \omega_{p,b}^2 \quad (1)$$

$$\sigma_{dc} = 4\pi\left[\omega_{p,n}^2\tau_n(T) + \omega_{p,b}^2\tau_b(T)\right] \quad (2)$$

where ω_p represents the plasma frequency, σ_{dc} is the dc conductivity, and τ is the mean scattering time. Here, the subscripts n and b indicate the Dirac band and semimetallic bands, respectively, responsible for narrow and broad Drude responses. The values of ω_p and σ_{dc} can be acquired from optical and transport experiments, respectively. Once one set of Drude parameters ($\omega_{p,b}$ and τ_b) has been obtained from the measured optical spectra, the remaining Drude parameters ($\omega_{p,n}$ and τ_n) can be necessarily determined from Eqs. (1) and (2). This approach will be extremely convenient when one of the Drude components has an absorption feature too sharp to measure reliably using conventional spectroscopic methods [15,16].

Optical properties in the mid- to near-IR region were also investigated via spectroscopic ellipsometry. Such an investigation is crucial for understanding fundamental electrodynamics of Dirac fermions, such as quantized universal absorption [25]. The influence of a SOI-induced gap on the electrodynamics would also be an interesting research topic. In addition, there should be a spectral weight due to the optical transition between semimetallic bands [15,16]. Thus, for more reliable study, the band structure should be identified based on mid- to near-IR optical properties, which in turn gives results consistent with the previous ARPES data.

II. METHODS: GROWTH, EXPERIMENTS, AND CALCULATIONS

Our $SrMnBi_2$ single crystals were grown using the Bi-flux method [18]. The dimensions of our single crystal were about 2 mm × 2 mm × 1 mm. The fresh surface of $SrMnBi_2$ was found to degrade within 1 h in air or 2 days at 10^{-8} mbar. Thus, for the optical measurements, the single crystals were cleaved and then immediately loaded into a high-vacuum cryostat unit to prevent surface contamination in the atmosphere. FTIR measurements were performed over photon energies $\hbar n$ below 1 eV [26]. For reference normalization, the reflectivity spectra $R(\omega)$ were measured repeatedly before and after *in situ* gold evaporation [27]. In the higher-energy region from 0.7 to 5 eV, we carried out spectroscopy ellipsometry measurements to obtain complex optical conductivity $\tilde{\sigma}(\omega) = \sigma_1(\omega) + i\sigma_2(\omega)$ directly. We obtained $\tilde{\sigma}(\omega)$ in the whole energy region by anchoring the higher-energy ellipsometry data [15,16]. The dc transport data were acquired via a six-probe method with a Physical Property Measurement System (PPMS-14T). For density functional theory (DFT) calculations, the full-potential linearized augmented plane-wave method was used, implemented in the WIEN2K package [28]. The generalized gradient approximation with the Perdew-Burke-Ernzerhof exchange-correlation potential was used for the DFT calculations [29].

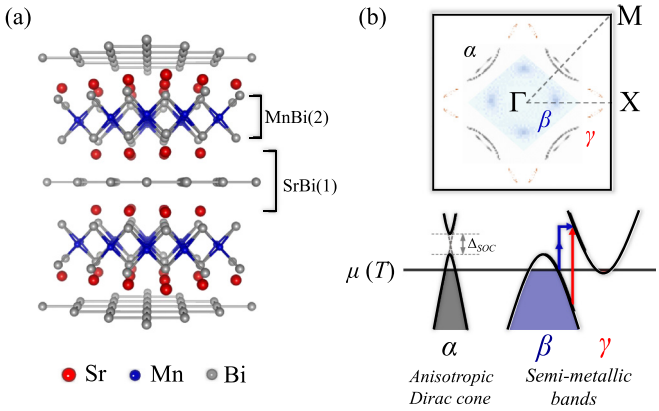

FIG. 1. (a) Crystal structure of $SrMnBi_2$, composed of a SrBi(1)-square net and an edge-shared MnBi(2) layer. (b) Schematic diagram of the electronic structure of $SrMnBi_2$ [bottom, based on band calculation (see Methods section), transport, and optical data], which possesses both an anisotropic Dirac cone (α) and semimetallic parabolic bands (β and γ). The constant energy surface [top, sliced at the Fermi level $\mu(T)$] consists of two hole pockets (α and β pockets), respectively, in the middle of the Γ-M line and near the Γ point, while an electron pocket (γ pocket) originates from near the X point. The Dirac-like state possesses a small energy gap Δ_{SOC} induced by sizable spin-orbit coupling (SOC). The semimetallic bands allow both direct and indirect optical transitions, represented by red and blue arrows in (b), respectively.

III. STRUCTURE: CRYSTAL (IN REAL SPACE) AND BAND (IN MOMENTUM SPACE)

The crystalline structure of $SrMnBi_2$ can be understood by considering two basis layers, as shown in Fig. 1(a) [17–24]. There is an array of $MnBi_4$ tetrahedrons connected in an edge-shared form, the so-called the MnBi(2) layer [17–24]. The Mn^{2+} ions in the MnBi(2) layer have a formal valence of 2+ [17,20]. As confirmed by a neutron-scattering study [19], the spins at the Mn^{2+} ions form an antiferromagnetic order along the c axis at the Néel temperature $T_N \approx 290$ K. Between pairs of MnBi(2) layers, a layer of Bi-square net exists as sandwiched by top and bottom layers of Sr ions, denoted by the SrBi(1) layer [17–20,23,24]. The quasi-two-dimensional (2D) Bi-square net, an unusual conducting channel, causes $SrMnBi_2$ to exhibit intriguing electronic structures near E_F [17,18,20,22,23].

$SrMnBi_2$ is known to be a novel bulk Dirac material that hosts a highly anisotropic Dirac conic state in the 2D Bi-square net [17,18,22,23]. As shown at the top of Fig. 1(b), the constant energy cut near E_F of our band calculation shows an α pocket in the middle of the $\Gamma - M$ direction in the Brillouin zone. The electronic band corresponding to the α pocket was found to have a linearly dispersive state with strong in-plane anisotropy [17,18,22,23]. The existence of such a Dirac-like state was confirmed in earlier ARPES [18,22,23] studies as well as predicted by first-principles calculations [17,18,20]. The α band in $SrMnBi_2$ is predominantly constructed based on $6p_x$ and $6p_y$ orbitals of Bi atoms [17–19,21,24], similar to the Dirac-like surface states in Bi-based topological insulators (Bi TIs) such as Bi_2Se_3 and Bi_2Te_3 [30,31]. In addition, the Dirac fermions in $SrMnBi_2$ mostly reside in the quasi-2D

Bi-square net [17,18,20,22,23]. Such 2D characteristics of free carriers are also reminiscent of the Dirac surface state in Bi TIs confined in the outermost surface layer [10,32–35]. However, the Dirac-like state in $SrMnBi_2$ is not necessarily localized on the surface (or at the boundary) but rather is distributed throughout the bulk in a discrete periodic pattern [17,18,20].

In addition to the highly anisotropic Dirac state, Fig. 1(b) shows that $SrMnBi_2$ has a hole-like β band near the Γ point and electronlike γ bands near the X point [17–20,22,23]. These valence and conduction bands have parabolic dispersions [17–20,22,23]. Hence, the entire electronic structure of $SrMnBi_2$ can be represented by the simple schematic diagram shown in the bottom of Fig. 1(b), where those bands (one linear and two parabolic) become involved. Therefore, the electrodynamic response of $SrMnBi_2$ should be more complicated than that of graphene, which is well described by a single Drude model [36,37]. At first sight, it seems to be appropriate to use a three-carrier model to describe the electrodynamics of $SrMnBi_2$, but such an analysis would require too many fitting variables.

We decided to use two-carrier model for the following reasons. Note that the existence of the γ pocket near the X point is quite subtle. Our calculation shows that the γ pocket provides a very small contribution to the Drude term due to its low doping. In fact, such a γ pocket was not observed in some of the previous ARPES reports [18,22,23]. Such a difference may come from the subtle dependence on the parameters in our calculation and small variation of doping in real samples. The small number of free carriers in the γ band, if they exist, does not make a significant contribution in free-carrier dynamics. Moreover, the scattering rates of carriers in both β and γ bands are much larger than that in the Dirac band, so the electrodynamics of β and γ bands can be treated approximately as an effective parabolic band. Thus, we can use a two-carrier model to describe the electrodynamics of $SrMnBi_2$: one from the anisotropic Dirac conic state and the other from the parabolic bands.

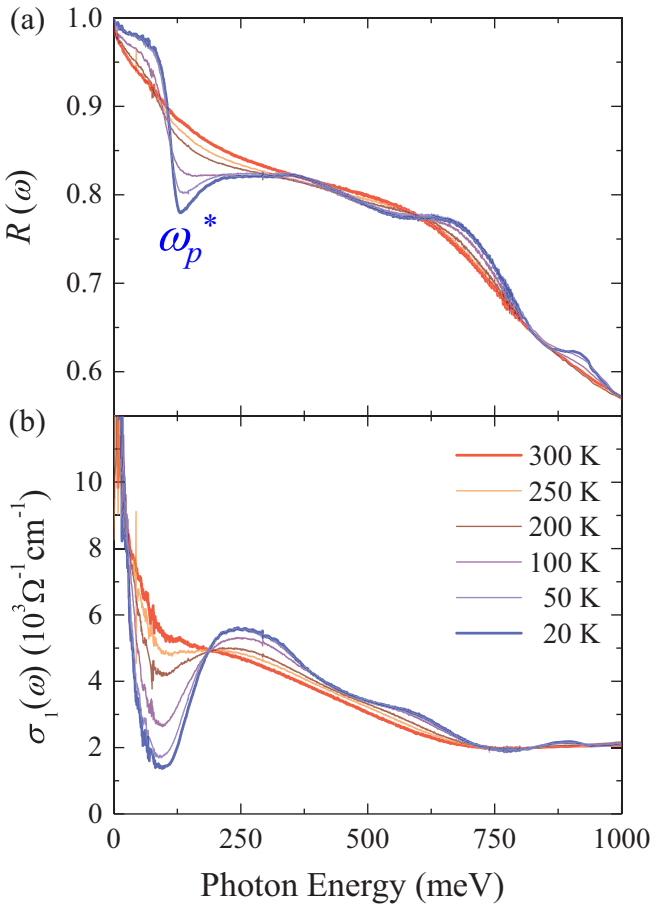

FIG. 2. (a) Temperature (T)-dependent evolution of reflectivity $R(\omega)$ and (b) the calculated optical conductivity $\sigma_1(\omega)$ spectra of $SrMnBi_2$ over the photon energies 7 − 1000 meV. The screened plasma frequency ω_p^*, a signature of metallic properties here, is presented at the dip in $R(\omega)$. The value of ω_p^* is well defined only in the low-T regime ($T < 100rmK$) and broadens out at higher T ($T > 100$ K). $\sigma_1(\omega)$ in (b) shows the free-carrier response in the low-energy (far-infrared, FIR) regime and the gaplike feature in the high-energy (mid-IR) region.

IV. EXPERIMENTAL DATA AND DISCUSSION

The measured reflectivity spectra $R(\omega)$ of our $SrMnBi_2$ single crystal showed the characteristic response of a semimetal. Figure 2(a) shows $R(\omega)$ at temperatures T from 20 to 300 K. In the far-infrared region (FIR) below 75 meV, $R(\omega)$ increased monotonically and finally approached unity at the low-frequency limit, following the Hagen-Rubens relation [15]. Simultaneously, a clear plasma-edge minimum was observed in $R(\omega)$ around 120 meV. These spectral features suggest the presence of free carriers in our $SrMnBi_2$ crystals for all T. However, the screened plasma frequency ω_p^* of $SrMnBi_2$ was only ∼120 meV, which is much lower than ∼5 eV typical for a metal. Since $\omega_p^2 = ne^2/m^*$, the number of free carriers is much smaller than for a typical metal, indicating the semimetallic nature of $SrMnBi_2$. Interestingly, as $\hbar\omega$ decreased in the low-energy regime, a soft increase in $R(\omega)$ at higher temperatures turned into a sudden increase below 100 K. This abrupt spectral change is quite intriguing. It is due to development of a very sharp Drude peak at low temperature, as we demonstrate later.

The optical conductivity spectra $\sigma_1(\omega)$ in Fig. 2(b) show the Drude response of the free carriers in the FIR region (i.e., below ∼75 meV) and a double-peak structure in the mid-IR (MIR) region. As T decreases, the Drude response gradually became sharper and a gaplike dip develops near 120 meV. At the same time, the spectral weight around 120 meV transferred into the higher-energy region, resulting in a double-peak structure in $\sigma_1(\omega)$ near 250 and 550 meV. It is notable that the double-peak structure did not exhibit a significant peak shift with increasing T; instead, an isosbestic point was observed at 190 meV, which has been observed in many strongly correlated electron systems [38–41]. It was also confirmed that the total spectral weight, acquired by integrating $\sigma_1(\omega,T)$, was nearly conserved over frequencies up to 750 meV. Satisfaction of the optical sum rule indicated that the T-dependent evolution of the optical responses comes mainly from redistributing the spectral weight below 750 meV [15,16].

Next we considered the low-energy electrodynamics of free carriers in view of the Drude term and plasma excitation. The value of $\sigma_1(\omega)$ in the low-energy region below 75 meV is plotted in Fig. 3(a), with the dc conductivity σ_{dc}

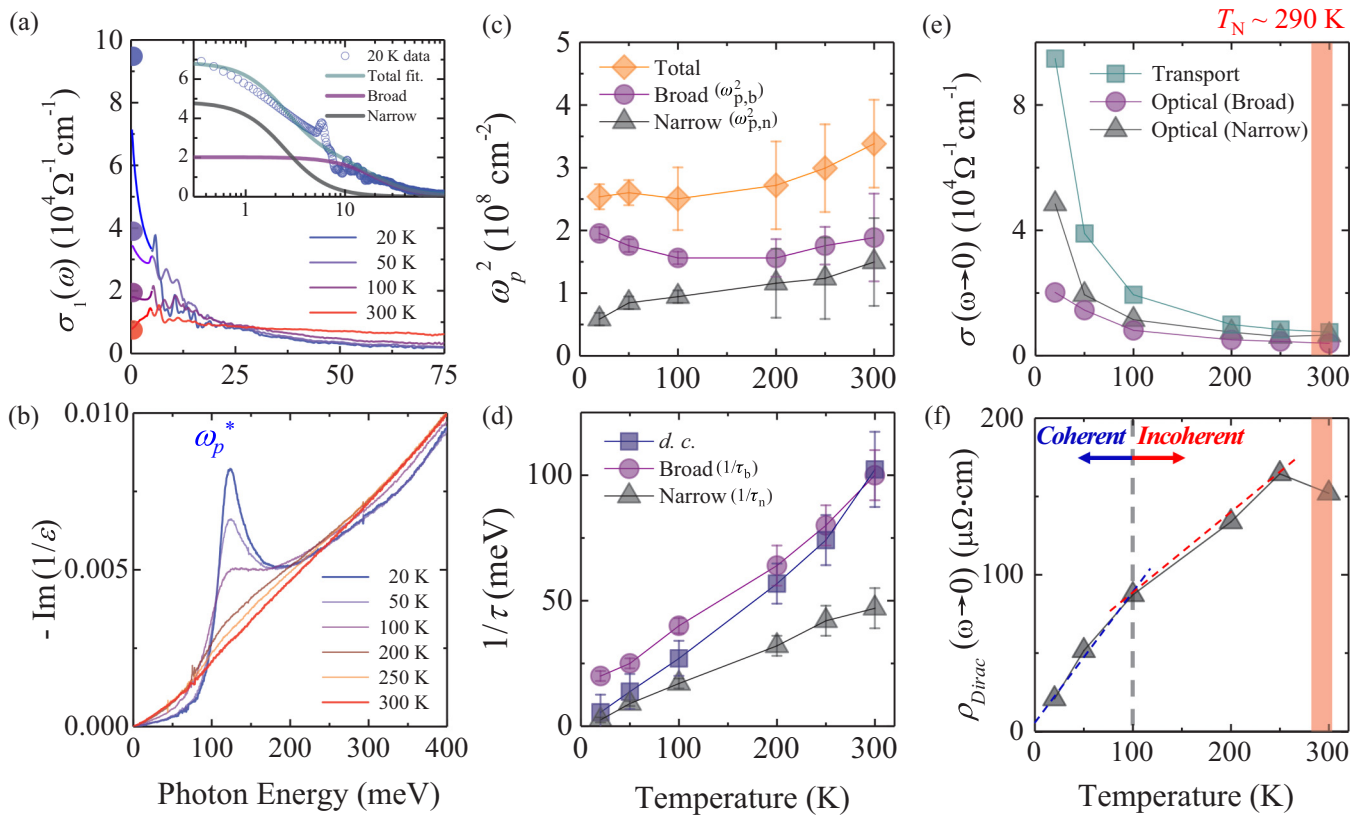

FIG. 3. (a) Temperature (T)-dependent change in the optical conductivity $\sigma_1(\omega)$ of $SrMnBi_2$ at low photon energies below 75 meV. The markers (solid circles) correspond to dc conductivity values measured from our complementary transport experiments. The inset in (a) shows the result of the two-carrier-model fit to our low-energy $\sigma_1(\omega)$, representatively performed on our 20-K data, giving rise to highly separable broad and narrow Drude features. (b) The peak in the energy-loss function $-\mathrm{Im}\{1/\hat{\varepsilon}(\omega)\}$ indicates the screened plasma frequency ω_p^* of $SrMnBi_2$. The value of $\omega_p^* \sim 120$ meV is much lower than that of a typical metal, suggesting its semimetallic nature. (c) The Drude spectral weight ${\omega_p}^2$ and (d) the scattering rate $1/\tau$ were extracted through the two-carrier-model fit. (e, f) T-dependent dc transport properties. As shown in (e), the dc transport conductivity σ_{dc} can be explained when the dc limits of optical conductivity $\sigma(\omega \to 0)$ for the Dirac and semimetallic Drude band contributions are included. The different transport behavior of both bands is evidenced, especially below $T = 100$ K. The overall T-linear behavior (with two distinct regimes) of the optical resistivity $\rho(\omega \to 0)$ for Dirac fermions in (f) implies the presence of strong electron-phonon interactions. In addition, the deviation (shaded red region) from the linear trend near $T_N \approx 290$ K presumably indicates the interplay between Dirac fermions and magnetism.

values acquired from our subsidiary transport measurements overlain. The individual $\sigma_1(\omega)$ spectra measured at a given T exhibited a clear free-carrier response in this spectral window [15,16]. At 300 K, the $\sigma_1(\omega)$ of free carriers can be represented approximately by a single broad Drude model; however, as T decreased, $\sigma_1(\omega)$ gradually split into both sharp and broad components. The inset of Fig. 3(a) shows that the value of $\sigma_1(\omega)$ at 20 K is well described by the linear sum of narrow and broad Drude components, with scattering rates of $1/\tau_n \sim 20\,\mathrm{cm}^{-1}(\approx 2.5\,\mathrm{meV})$ and $1/\tau_b \sim 160\,\mathrm{cm}^{-1}(\approx 20\,\mathrm{meV})$, respectively. Here, the narrow Drude term is mandated by the standard extrapolation technique to dc conductivity [15,16]. The substantial T-dependent change in the Drude response can also be verified by the evolution of the peak in the energy-loss function $-\mathrm{Im}(1/\varepsilon(\omega))$ in Fig. 3(b). At 20 K, a sharp plasma excitation, which is a signature of metallicity, was observed at $\omega_p^* \sim 120$ meV. With increasing T, the spectral feature broadened significantly, becoming barely noticeable above 200 K. This spectral change in $-\mathrm{Im}(1/\varepsilon(\omega))$ is closely related to the observed large change in $R(\omega)$ near the plasma-edge minimum at low T [Fig. 2(a)].

It should be noted that the narrow component is necessary to fill the spectral weight below 25 meV which is notably missing otherwise. Note that the scattering rate of the narrow Drude term at $T = 20$ K is smaller than the lowest frequency of our reliable measurement window [26]. However, the narrow component term is indispensable to resolve the discrepancy between σ_{dc} and the dc limit of $\sigma_1(\omega)$, which is shown in Fig. 3(e). Our two-carrier model analysis given in Eqs. (1) and (2) strongly supports the presence of such a conducting channel characterized by an extremely low scattering rate. The resulting value of $1/\tau_n \sim 20\,\mathrm{cm}^{-1}(2.5\,\mathrm{meV})$ at 20 K is comparable with that of Bi TIs when measured at room temperature [35]. In comparison to Bi TIs, the slightly large value of $1/\tau$ for Dirac fermions in $SrMnBi_2$ may originate from the SOI-induced gap in the Dirac-like state [17–24]. Here we note that the entire Drude feature possibly can be fitted by a single Drude model with a broad incoherent sideband, often observed in heavy fermion systems [42]. Note that, for $SrMnBi_2$, we have two distinct origins responsible for the Drude response, according to the band structure shown in Fig. 1(b) and the literature [18,22,23]. In addition, Hall

measurement data from the literature, identifying the presence of two distinct types of carriers in $SrMnBi_2$, strongly support our two-carrier-model analysis of $\sigma_1(\omega)$ [21].

Here, we assign the narrow Drude peak to the optical absorption of Dirac fermions in the Bi(1)-square net, corresponding to the α pocket in Fig. 1(b). Basically, this takes into account conventional transport properties, such as the low scattering rate and high mobility of Dirac fermions [3,17,35]. For $SrMnBi_2$, such superb transport properties arise from pseudospin conservation under time-reversal symmetry [17]. The two-carrier-model analysis allows us to isolate $\omega_{p,n}^2$ and $1/\tau_n$ for pure Dirac fermions in $SrMnBi_2$, as shown in Figs. 3(c) and 3(d), respectively. As T increased, $\omega_{p,n}^2$ increased sharply below 100 K and gently up to 300 K, while $1/\tau_n$ increased almost linearly with T. In contrast, the Drude weight for the broad component $\omega_{p,b}^2$ remained more or less constant as T decreased to 100 K, while a clear upturn appeared below 100 K [Fig. 3(c)]. For the Drude weight of the narrow component $\omega_{p,n}^2$, which exhibits a monotonic decrease at low T, the total ω_p^2 remained nearly conserved over all values of T, particularly below 200 K. The T dependence of $\omega_{p,b}^2$ possibly originates from two factors, namely, the semimetallic band structure and the small density of states (DOS) near E_F in our $SrMnBi_2$ sample. With a small DOS at E_F, the chemical potential $\mu(T)$ can shift fairly far along the T variation [43]. Thus, we expected T-dependent changes in the carrier density and a subsequent T evolution of $\omega_{p,b}^2$.

The small $1/\tau$ of the Dirac fermions at low T will govern the transport properties in the corresponding T range. Figure 3(d) shows the values of $1/\tau$ acquired from the two-carrier-model fit to $\sigma_1(\omega)$. For comparison, we also calculated the dc scattering rate $1/\tau_{dc} = \rho_{dc}(T){\omega_p}^2$ with $\rho_{dc}(T)$ obtained from our transport measurements. Below 100 K, the value of $1/\tau_{dc}$ approached $1/\tau$ of the narrow Drude term. In the same T range, the $1/\tau$ value of the broad Drude peak was about eight times larger than that of the narrow one. Thus, low-T carrier transport is governed by the free carriers responsible for the narrow Drude term. On the other hand, at higher T, $1/\tau_{dc}$ gradually increased and converged to that of the broad Drude terms. The results imply that the narrow and broad Drude components serve as the predominant transport carriers at low and high T, respectively. Note that all values of $1/\tau$ shown in Fig. 3(d) exhibit nearly linear behavior over the wide T range.

From the narrow Drude response at 20 K, we calculated the mobility of Dirac fermions in $SrMnBi_2$, which was found to reach $\mu = e\tau/m^* \sim 1600\,\mathrm{cm}^2/(\mathrm{V\,s})$, and a Dirac fermion density of around $n \sim 1.8 \times 10^{20}\,\mathrm{cm}^{-3}$. For this estimation, an effective mass $m^*/m_e \approx 0.29$ of Dirac fermions in $SrMnBi_2$ was adopted from Shubnikov–de Haas oscillations measured at 20 K [18]. The results were consistent with the Hall measurement data in [21], especially the mobility of $\mu \sim 1950\,\mathrm{cm}^2/(\mathrm{Vs})$ for Dirac fermions in $SrMnBi_2$. With the dc limit of optical conductivity presented in Fig. 3(e), we confirmed that our analysis technique is capable of isolating Dirac fermions from the mixed response, which is generally impossible using only the transport data (without external magnetic field $\boldsymbol{H}$) shown in Fig. 3(f). The success in the separation of Dirac fermions with no external $\boldsymbol{H}$ implies the usefulness of our two-carrier-model analysis.

Our electrodynamic studies demonstrate that the small values of $1/\tau_n$ play important roles in determining the transport properties at low temperature. As shown in Fig. 3(f), the dc limit of resistivity ρ, obtained by taking the low-frequency limit of the narrow Drude conductivity, has an overall linear T dependence, except at 300 K [44]. We attribute that the linear T dependence might come from the strong e-ph interaction in the 2D low-carrier-density system $SrMnBi_2$. As noted for graphene [45], ρ exhibits a quasiclassical T-linear (not T^4) behavior well below the Debye temperature Θ_D ($\Theta_D = 310$ K for $SrMnBi_2$ [46]). Similar to graphene, $1/\tau$ for Dirac fermions in $SrMnBi_2$ is also linear in T, as shown in Fig. 3(d). However, in comparison with graphene [3], $1/\tau$ for Dirac fermions in $SrMnBi_2$ has a much steeper slope. This result indicates that the Dirac fermions in $SrMnBi_2$ are under the influence of strong e-ph interaction.

The key parameter for assigning such a strong e-ph interaction to the Dirac fermions in $SrMnBi_2$ would be spatial overlap between orbitals (electrons) and bonds (phonons). Essentially, the Dirac fermions in $SrMnBi_2$ predominantly reside in the in-plane p_x and p_y orbitals [17–19,21,24] while they reside in the out-of-plane p_z orbital for graphene. Accordingly, the Dirac fermions in $SrMnBi_2$ form a huge density overlap with in-plane Bi(1) ions, giving rise to strong Coulomb interactions in between; this naturally leads to strong e-ph interaction in $SrMnBi_2$. In contrast, the Dirac fermions in graphene have nearly zero density along the C-C bond and, thus, have only a weak e-ph interaction. This scenario can be substantiated in the case of graphene in which the e-ph interaction in the σ (in-plane orbital) band is several orders of magnitude greater than that in the π (out-of-plane orbital) band [47–49]. Electron-magnon coupling may possibly form scattering channels; however, the contribution of this mechanism may be negligible, as explained in [50].

Such strong e-ph interactions cause incoherent transport of Dirac fermions. As shown by both our transport data [shown in Fig. 3(f)] and values from the literature [21], the mobility of Dirac fermions in $SrMnBi_2$ drastically decreases with increasing T. This behavior differs considerably from the case of graphene in which the Dirac fermions with high mobility survive up to room temperature [2,51,52]. Our optical measurement data provide further decisive evidence for this incoherence, showing a noticeable increase in $1/\tau$ at high T, as shown in Fig. 3(d), and a decrease in $d\rho_{Dirac}(\omega \to 0)/dT$, which corresponds to the slope of $\rho_{Dirac}(\omega \to 0)$ in Fig. 3(f). In particular, the value of $1/\tau$ is related to the mobility through the relation $\mu = e\tau/m^*$, where e is the elementary charge and m^* the effective mass of carriers; $1/\tau$ for Dirac fermions in $SrMnBi_2$ shows a 20-fold increase as T increases from 20 K to 300 K. Additionally, for the values of $\sigma_1(\omega)$ at room temperature presented in Fig. 3(a), the Drude response showed flat absorption below 100 meV, with no clear hallmark of Dirac fermions, and a downturn was observed below 10 meV. These changes in the optical data at high T correspond to the typical signature of incoherent transport of highly overdamped Dirac quasiparticles due to significant scattering processes [15,42,53,54].

Next, we consider the seemingly optical-gap-like feature observed in $\sigma_1(\omega)$ at low T, which becomes gradually filled as

T increases. The T-dependent spectral evolution is similar to that due to spin-density-wave (SDW) formation in iron pnictide superconductors [55–58]. For example, dramatic spectral evolutions have been reported for various iron pnictides across the SDW transition below T_N [55–58]. The optical spectra of $SrMnBi_2$ and its T evolution appear qualitatively similar to those of iron pnictides, specifically, the decrease of $1/\tau$, the gap opening in the MIR region below T_N, and the transfer of the spectral weight near the gap into the high-frequency region. However, we cannot attribute the gaplike feature to SDW formation in $SrMnBi_2$. According to the SDW scenario, both ω_p^2 and $1/\tau$ decrease drastically just below T_N, exhibiting a kink in ρ at T_N [59]. Instead, we observed a gradual change of ω_p^2, $1/\tau$, and ρ (T) with decreasing T. Additionally, the MIR peak shift is not sufficient to apply the SDW scenario, which predicts a systematic increase of the gap size below T_N. Moreover, the expected, $2\Delta/k_BT_N$ values are about 10 and 25, which are significantly larger than those found for conventional SDW materials [55,60,61]. Thus, the origin of the gaplike feature should be attributed to another mechanism.

Figure 4(a) shows the T-dependent residual $\sigma_1(\omega)$ of $SrMnBi_2$ after subtracting the free-carrier absorption. According to optical studies on graphene or graphite, their optical spectra include a frequency-independent universal conductance in the MIR region, which can be ascribed to both the two-dimensionality and the linear dispersion of the Dirac band [62,63]. We would expect such an optical feature for our case of the anisotropic Dirac band in $SrMnBi_2$. In fact, the broad flat background above $\hbar\omega = 2E_F$ ($\approx$120 meV in our case) may be relevant to universal absorption in $SrMnBi_2$. The absorption edge becomes blunt with increasing T due to the thermal redistribution of Dirac fermions [64–66]; the additional gaplike and peak structures in the spectra will be dominated by the contribution from the semimetallic bands in the MnBi(2) layer. The theoretical values of $\sigma_1(\omega)$ obtained from DFT calculations at 0 K are also plotted in Fig. 4(a), for comparison with our optical data. The calculated $\sigma_1(\omega)$ was renormalized by a factor of $Z = 0.59$ for comparison of values on the same scale; such scaling may be required due to the strong correlation in Mn $3d$ electrons. All of the peak positions were, overall, in good agreement with the calculations.

To understand the origin of the gaplike and peak structures in $\sigma_1(\omega)$, the band structure along the M-Γ-X direction is shown in Fig. 4(b), and the partial density of states (PDOS) in Fig. 4(c). In the calculation results, the semimetallic band does not appear to cross E_F along the given direction, distinct from the band schematic shown in Fig. 1(b). The difference originates from the fact that optical spectroscopy can reflect the response, which is not selected along a specific direction but integrated over the entire k space. Nevertheless, we can resolve the high-energy optical transitions based on our calculation results without loss of generality. Figure 4(b) shows the electronic states responsible for the low-energy ($\sim$250 meV; red) and high-energy ($\sim$550 meV; blue) optical transitions, as denoted by the arrows in Fig. 4(c). Both optical transitions give rise to the double-peak structure in the $\sigma_1(\omega)$ spectra. In addition, the bent arrow in Fig. 4(b) indicates possible indirect phonon-assisted transitions [67], which can lead to the gap-filling process observed in $\sigma_1(\omega)$ at high T. At high T, there

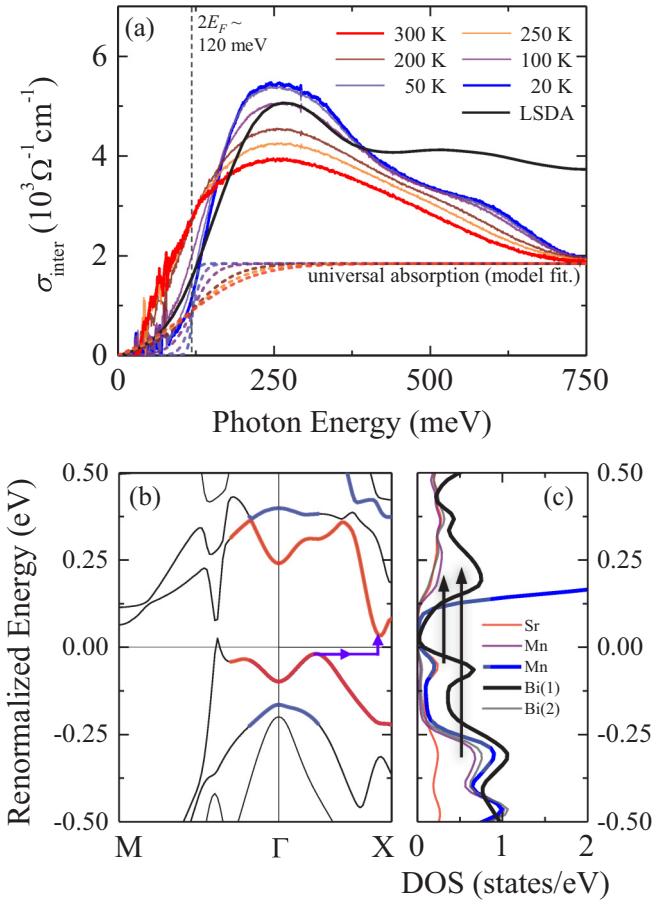

FIG. 4. (a) Optical conductivity $\sigma_{1,\text{inter}}(\omega)$ spectra dominated by the interband transitions after excluding the free-carrier contribution from the entire conductivity $\sigma_1(\omega)$. The theoretical $\sigma_{1,\text{inter}}(\omega)$ at $T = 0$ K (labeled by LSDA, a black solid line) was also obtained from density functional calculations with band renormalization by a factor of $Z = 0.59$. Here, the dashed background shows our estimation for the universal absorption expected for the Dirac state. The absorption edge is less pronounced as T increases due to thermal redistribution of the Dirac fermion population. (b) The band structure along the M-Γ-X direction includes both the linear Dirac-conic (along the M-Γ) and parabolic semimetallic bands (Γ-X). The electronic bands relevant for direct interband transitions are represented by both the red and blue lines while a blue arrow indicates the indirect interband transition possibly assisted by phonons at high T. (c) The partial density of states (PDOS) integrated over k space also identifies the optical interband transitions (represented by two black arrows), corresponding to the double-peak structure in the $\sigma_{1,\text{inter}}(\omega)$.

is a sufficient phonon population to open the phonon-assisted indirect transition channels, with an accompanying transfer of spectral weight from the higher-lying double peak into the lower-lying gaplike dip. As T decreases (and, thus, the phonon population diminishes), phonon-assisted transitions will be suppressed, leading to the prominent gaplike feature in $\sigma_1(\omega)$ at low T. From this analysis, one can understand the gap- and peaklike features in the $\sigma_1(\omega)$ distribution for $SrMnBi_2$ and their spectral weight transfer, which are often observed in various semiconductors or semimetals with an indirect band gap [68,69].

V. CONCLUSION

In this study, we separated the optical response of free carriers in $SrMnBi_2$ through a two-carrier-model analysis: Dirac fermions in the Bi(1)-square net and non-Dirac fermions in the semimetallic MnBi(2) layer. This analysis provides a unique opportunity to investigate the low-energy electrodynamics of Dirac fermions. The determinants of the transport properties of Dirac fermions were comprehensively addressed, including pseudospin, spin-orbit interaction, magnetism, and *e-ph* interactions. In sharp contrast to graphene, Dirac fermions dominated the transport only at low temperatures but gradually became incoherent as the temperature increased due to strong electron-phonon coupling. In the mid-IR region, we identified a seemingly optical-gap-like feature that appeared at low temperatures but gradually filled in with increasing temperature. This gap-filling behavior can be ascribed to indirect phonon-assisted optical transitions.

ACKNOWLEDGMENTS

We acknowledge valuable discussions with H. S. Jin, J. H. Bae, M. Kim, J. S. Hwang, C. H. Park, H. Min, Y.-W. Son, and K. Burch. This work was supported by the Institute for Basic Science (IBS) in Korea (IBS-R009-D1). J.S.K. was supported by the National Research Foundation (NRF) of Korea through SRC (Grant No. 2011-0030785), the Max Planck POSTECH/KOREA Research Initiative (Grant No. 2016K1A4A4A01922028) programs. S.J.M., K.W.K., and D.-Y.C. were supported by the Basic Science Research Program through the NRF of Korea funded by the Ministry of Science, ICT, & Future Planning (Grants No. 2017R1A2B4009413, No. 2015R1A2A1A10056200, and No. 2015R1C1A1A02037514, respectively). J.H.S. was supported by the Radiation Technology R&D Program through the NRF of Korea (2017M2B2A9072831).

H.J.P. and B.C.P. contributed equally to this work.

[1] K. S. Novoselov, A. K. Geim, S. V. Morozov, D. Jiang, Y. Zhang, S. V. Dubonos, I. V. Grigorieva, and A. A. Firsov, Science **306**, 666 (2004).

[2] A. H. Castro Neto, F. Guinea, N. M. R. Peres, K. S. Novoselov, and A. K. Geim, Rev. Mod. Phys. **81**, 109 (2009).

[3] S. Das Sarma, S. Adam, E. H. Hwang, and E. Rossi, Rev. Mod. Phys. **83**, 407 (2011).

[4] M. König, S. Wiedmann, C. Brune, A. Roth, H. Buhmann, L. W. Molenkamp, X.-L. Qi, and S.-C. Zhang, Science **318**, 766 (2007).

[5] M. Z. Hasan and C. L. Kane, Rev. Mod. Phys. **82**, 3045 (2010).

[6] X. L. Qi and S. C. Zhang, Rev. Mod. Phys. **83**, 1057 (2011).

[7] Z. Q. Li, E. A. Henriksen, Z. Jiang, Z. Hao, M. C. Martin, P. Kim, H. L. Stormer, and D. N. Basov, Nat. Phys. **4**, 532 (2008).

[8] Y. B. Zhang, Y. W. Tan, H. L. Stormer, and P. Kim, Nature (London) **438**, 201 (2005).

[9] C. Z. Chang, J. S. Zhang, X. Feng, J. Shen, Z. C. Zhang, M. H. Guo, K. Li, Y. B. Ou, P. Wei, L. L. Wang, Z. Q. Ji, Y. Feng, S. H. Ji, X. Chen, J. F. Jia, X. Dai, Z. Fang, S.-C. Zhang, K. He, Y. Y. Wang, L. Lu, X. C. Ma, and Q. K. Xue, Science **340**, 167 (2013).

[10] Y. Xu, I. Miotkowski, C. Liu, J. Tian, H. Nam, N. Alidoust, J. Hu, C.-K. Shih, M. Z. Hasan, and Y. P. Chen, Nat. Phys. **10**, 956 (2014).

[11] J. G. Checkelsky, R. Yoshimi, A. Tsukazaki, K. S. Takahashi, Y. Kozuka, J. Falson, M. Kawasaki, and Y. Tokura, Nat. Phys. **10**, 731 (2014).

[12] M. Mogi, M. Kawamura, R. Yoshimi, A. Tsukazaki, Y. Kozuka, K. S. Takahashi, M. Kawasaki, and Y. Tokura, Nat. Mater. **16**, 516 (2017).

[13] K. S. Novoselov, V. I. Fal, L. Colombo, P. R. Gellert, M. G. Schwab, K. Kim, V. I. Fal'ko, L. Colombo, P. R. Gellert, M. G. Schwab, and K. Kim, Nature (London) **490**, 192 (2013).

[14] P. Avouris, Z. Chen, and V. Perebeinos, Nat. Nanotechnol. **2**, 605 (2007).

[15] M. Dressel and G. Gruner, *Electrodynamics of Solids* (Cambridge University Press, Cambridge, UK, 2002).

[16] D. N. Basov, R. D. Averitt, D. van der Marel, M. Dressel, and K. Haule, Rev. Mod. Phys. **83**, 471 (2011).

[17] G. Lee, M. A. Farhan, J. S. Kim, and J. H. Shim, Phys. Rev. B **87**, 245104 (2013).

[18] J. Park, G. Lee, F. Wolff-Fabris, Y. Y. Koh, M. J. Eom, Y. K. Kim, M. A. Farhan, Y. J. Jo, C. Kim, J. H. Shim, and J. S. Kim, Phys. Rev. Lett. **107**, 126402 (2011).

[19] Y. F. Guo, A. J. Princep, X. Zhang, P. Manuel, D. Khalyavin, I. I. Mazin, Y. G. Shi, and A. T. Boothroyd, Phys. Rev. B **90**, 075120 (2014).

[20] J. K. Wang, L. L. Zhao, Q. Yin, G. Kotliar, M. S. Kim, M. C. Aronson, and E. Morosan, Phys. Rev. B **84**, 064428 (2011).

[21] K. Wang, D. Graf, H. Lei, S. W. Tozer, and C. Petrovic, Phys. Rev. B **84**, 220401 (2011).

[22] Y. Feng, Z. Wang, C. Chen, Y. Shi, Z. Xie, H. Yi, A. Liang, S. He, J. He, Y. Peng, X. Liu, Y. Liu, L. Zhao, G. Liu, X. Dong, J. Zhang, C. Chen, Z. Xu, X. Dai, Z. Fang, and X. J. Zhou, Sci. Rep. **4**, 5385 (2014).

[23] L. L. Jia, Z. H. Liu, Y. P. Cai, T. Qian, X. P. Wang, H. Miao, P. Richard, Y. G. Zhao, Y. Li, D. M. Wang, J. B. He, M. Shi, G. F. Chen, H. Ding, and S. C. Wang, Phys. Rev. B **90**, 035133 (2014).

[24] A. Zhang, C. Liu, C. Yi, G. Zhao, T. Xia, J. Ji, Y. Shi, R. Yu, X. Wang, C. Chen, and Q. Zhang, Nat. Commun. **7**, 13833 (2016).

[25] R. R. Nair, P. Blake, A. N. Grigorenko, K. S. Novoselov, T. J. Booth, T. Stauber, N. M. R. Peres, and A. K. Geim, Science **320**, 1308 (2008).

[26] The experimental data are highly reliable between $E = 0.007$ and $E = 1.0$ eV. Below 0.007 eV, our optical spectra become quite noisy due to smallness of the light intensity from a blackbody radiation source and bolometer detection limit. In spite of the noise, our reflectivity spectra follow the Hagen-Rubens relation reasonably well with measured dc conductivity.

[27] C. C. Homes, M. Reedyk, D. A. Cradles, and T. Timusk, Appl. Opt. **32**, 2976 (1993).

[28] K. S. P. Blaha, G. K. H. Madsen, D. Kvasnicka, and J. Luitz, *WIEN2K, An Augmented Plane Wave + Local Orbitals Program for Calculating Crystal Properties* (Technische Universität, Wien, Austria, 2001).

[29] J. P. J. Perdew, K. Burke, and M. Ernzerhof, Phys. Rev. Lett. **77**, 3865 (1996).

[30] H. Zhang, C.-X. Liu, X.-L. Qi, X. Dai, Z. Fang, and S.-C. Zhang, Nat. Phys. **5**, 438 (2009).
[31] D. Hsieh, D. Qian, L. Wray, Y. Xia, Y. S. Hor, R. J. Cava, and M. Z. Hasan, Nature (London) **452**, 970 (2008).
[32] J. G. Analytis, R. D. McDonald, S. C. Riggs, J. H. Chu, G. S. Boebinger, and I. R. Fisher, Nat. Phys. **6**, 960 (2010).
[33] Y. Xu, I. Miotkowski, and Y. P. Chen, Nat. Commun. **7**, 11434 (2016).
[34] Y. Zhang, K. He, C.-Z. Chang, C.-L. Song, L.-L. Wang, X. Chen, J.-F. Jia, Z. Fang, X. Dai, W.-Y. Shan, S.-Q. Shen, Q. Niu, X.-L. Qi, S.-C. Zhang, X.-C. Ma, and Q.-K. Xue, Nat. Phys. **6**, 584 (2010).
[35] B. C. Park, T.-H. Kim, K. I. Sim, B. Kang, J. W. Kim, B. Cho, K. H. Jeong, M.-H. Cho, and J. H. Kim, Nat. Commun. **6**, 6552 (2015).
[36] J. Horng, C. F. Chen, B. Geng, C. Girit, Y. Zhang, Z. Hao, H. A. Bechtel, M. Martin, A. Zettl, M. F. Crommie, Y. R. Shen, and F. Wang, Phys. Rev. B **83**, 165113 (2011).
[37] K. F. Mak, M. Y. Sfeir, Y. Wu, C. H. Lui, J. A. Misewich, and T. F. Heinz, Phys. Rev. Lett. **101**, 196405 (2008).
[38] T. Katsufuji, Y. Okimoto, and Y. Tokura, Phys. Rev. Lett. **75**, 3497 (1995).
[39] Y. Tokura, Y. Okimoto, S. Yamaguchi, H. Taniguchi, T. Kimura, and H. Takagi, Phys. Rev. B **58**, R1699 (1998).
[40] J. S. Lee, Y. S. Lee, K. W. Kim, T. W. Noh, J. Yu, T. Takeda, and R. Kanno, Phys. Rev. B **64**, 165108 (2001).
[41] M. M. Qazilbash, M. Brehm, B. G. Chae, P.-C. Ho, G. O. Andreev, B. J. Kim, S. Y. Yun, A. V. Balatsky, M. B. Maple, F. Keilmann, H. T. Kim, and D. N. Basov, Science **318**, 1750 (2007).
[42] P. E. Jönsson, K. Takenaka, S. Niitaka, T. Sasagawa, S. Sugai, and H. Takagi, Phys. Rev. Lett. **99**, 167402 (2007).
[43] The chemical potential change with temperature is proportional to $-T^2N'(E_F)/N(E_F)$); J. M. Ziman, *Principles of the Theory of Solids* (Cambridge University Press, Cambridge, UK, 1965).
[44] The deviation from the linear trend between 250 and 300 K is probably related to the antiferromagnetic (AFM) order known to be formed around 290 K, which was confirmed by a neutron-scattering study [19]. The locally broken time-reversal symmetry due to antiferromagnetism may allow Dirac fermions to be backscattered.
[45] D. K. Efetov and P. Kim, Phys. Rev. Lett. **105**, 256805 (2010).
[46] K. Wang, L. Wang, and C. Petrovic, Appl. Phys. Lett. **100**, 112111 (2012).
[47] S. Ulstrup, M. Bianchi, R. Hatch, D. Guan, A. Baraldi, D. Alfe, L. Hornekaer, and P. Hofmann, Phys. Rev. B **86**, 161402(R) (2012).
[48] F. Mazzola, J. W. Wells, R. Yakimova, S. Ulstrup, J. A. Miwa, R. Balog, M. Bianchi, M. Leandersson, J. Adell, P. Hofmann, and T. Balasubramanian, Phys. Rev. Lett. **111**, 216806 (2013).
[49] J. C. Johannsen, S. Ulstrup, M. Bianchi, R. Hatch, D. Guan, F. Mazzola, L. Horneaer, F. Fromm, C. Raidel, T. Seyller, and P. Hofmann, J. Phys.: Condens. Matter **25**, 094001 (2013).
[50] Generally, the AFM order is achieved with Mn 3*d* electrons. Thus, to have strong electron-magnon coupling between the Dirac fermions and the AFM order, there should be large hybridizations between the Bi(1) 6*p* and the Mn 3*d* electrons. However, this is difficult to obtain, because the distance between the Bi(1) and the Mn ions is rather large (5.78 Å). DFT calculations show that the PDOS at the E_F of the Bi(2) 6*p* state in the MnBi(2) layer is very small (4.1%), while the PDOS of the Mn 3*d* states is considerable (22%) [17]. Because the effective hybridization between the Bi(1) 6*p* and the Mn 3*d* states will take place via the Bi(2) 6*p* state, it should be very weak. Thus, the electron-magnon coupling might be negligible for the Dirac fermions in the Bi(1)-square net. Actually, there is no resistivity anomaly at T_N [18]. Note that in a similar layered system $PdCrO_2$, in which a metallic Pd layer has a strong magnetic coupling with an insulating AFM CrO_2 layer [H.-J. Noh *et al.*, Sci. Rep. **4**, 3680 (2014)], a kinky structure was observed in the resistivity at T_N [H. Takatsu and Y. Maeno, J. Cryst. Growth **312**, 3461 (2010)].
[51] K. S. Novoselov, Z. Jiang, Y. Zhang, S. V. Morozov, H. L. Stormer, U. Zeitler, J. C. Maan, G. S. Boebinger, P. Kim, and A. K. Geim, Science. **315**, 1379 (2007).
[52] Y. W. Tan, Y. Zhang, K. Bolotin, Y. Zhao, S. Adam, E. H. Hwang, S. Das Sarma, H. L. Stormer, and P. Kim, Phys. Rev. Lett. **99**, 246803 (2007).
[53] P. Kostic, Y. Okada, N. C. Collins, Z. Schlesinger, J. W. Reiner, L. Klein, A. Kapitulnik, T. H. Geballe, and M. R. Beasley, Phys. Rev. Lett. **81**, 2498 (1998).
[54] Y. M. Dai, B. Xu, B. Shen, H. Xiao, H. H. Wen, X. G. Qiu, C. C. Homes, and R. P. S. M. Lobo, Phys. Rev. Lett. **111**, 117001 (2013).
[55] W. Z. Hu, J. Dong, G. Li, Z. Li, P. Zheng, G. F. Chen, J. L. Luo, and N. L. Wang, Phys. Rev. Lett. **101**, 257005 (2008).
[56] A. Charnukha, P. Popovich, Y. Matiks, D. L. Sun, C. T. Lin, A. N. Yaresko, B. Keimer, and A. V. Boris, Nat. Commun. **2**, 219 (2011).
[57] M. M. Qazilbash, J. J. Hamlin, R. E. Baumbach, L. Zhang, D. J. Singh, M. B. Maple, and D. N. Basov, Nat. Phys. **5**, 647 (2009).
[58] K. W. Kim, A. Pashkin, H. Schäfer, M. Beyer, M. Porer, T. Wolf, C. Bernhard, J. Demsar, R. Huber, and A. Leitenstorfer, Nat. Mater. **11**, 497 (2012).
[59] G. Grüner, *Density Waves in Solids* (Addison-Wesley, Reading, MA, 1994), Vol. 89.
[60] G. Grüner, Rev. Mod. Phys. **66**, 1 (1994).
[61] S. J. Moon, J. H. Shin, D. Parker, W. S. Choi, I. I. Mazin, Y. S. Lee, J. Y. Kim, N. H. Sung, B. K. Cho, S. H. Khim, J. S. Kim, K. H. Kim, and T. W. Noh, Phys. Rev. B **81**, 205114 (2010).
[62] T. Ando, Y. Zheng, and H. Suzuura, J. Phys. Soc. Jpn. **71**, 1318 (2002).
[63] A. B. Kuzmenko, E. van Heumen, F. Carbone, and D. van der Marel, Phys. Rev. Lett. **100**, 117401 (2008).
[64] S. Winnerl, M. Orlita, P. Plochocka, P. Kossacki, M. Potemski, T. Winzer, E. Malic, A. Knorr, M. Sprinkle, C. Berger, W. A. de Heer, H. Schneider, and M. Helm, Phys. Rev. Lett. **107**, 237401 (2011).
[65] Here, we estimate the Fermi energy $E_F \approx 60$ meV, through the Dirac model fit [66] to narrow Drude component $\sigma_{1,n}(\omega)$ at 20 K, the lowest T in our optical experiments.
[66] A. J. Frenzel, C. H. Lui, Y. C. Shin, J. Kong, and N. Gedik, Phys. Rev. Lett. **113**, 056602 (2014).
[67] H. J. Park, L. J. Sandilands, J. S. You, H. S. Ji, C. H. Sohn, J. W. Han, S. J. Moon, K. W. Kim, J. H. Shim, J. S. Kim, and T. W. Noh, Phys. Rev. B **93**, 205122 (2016).
[68] B. K. Sun, X. Zhang, and C. P. Grigoropoulos, Int. J. Heat Mass Transf. **40**, 1591 (1997).
[69] H. Y. Fan, Rep. Prog. Phys. **19**, 107 (1956).